

# Spontaneous imbibition in a porous medium under longitudinal temperature gradients

M. Sánchez and A. Medina

*Grupo de Medios Porosos y Granulados,  
Programa de Matemáticas Aplicadas y Computación, IMP  
Eje Central Lázaro Cárdenas #152, 07730 México D.F., México*

A. Rojano

*Programa Universitario de Investigación en Matemáticas,  
Estadística y Computación Inteligente, Universidad Autónoma Chapingo,  
56230 Chapingo, México*

Recibido el 22 de marzo de 2004; aceptado el 27 de junio de 2005

In this work, the influence of a longitudinal temperature gradient on the spontaneous imbibition into a homogeneous porous medium has been analyzed. Theory and experiments done on a permeable rock (Berea sandstone) allow us to show how this gradient modifies the temporal evolution of the averaged imbibition front  $h(t)$ . Despite the existence of a thermal boundary layer outside the rock, experimental data are in good agreement with the theoretical profiles of  $h(t)$ .

*Keywords:* Imbibition; Flow through porous media; Heat flow in porous media; Surface-tension-driven instability.

En este trabajo se analiza la influencia de un gradiente de temperatura longitudinal sobre la imbibición espontánea en un medio poroso homogéneo. La teoría y los experimentos hechos en una roca permeable (arenisca Berea) permiten mostrar cómo este gradiente modifica la evolución temporal del frente promedio de imbibición  $h(t)$ . A pesar de la existencia de una capa límite térmica fuera de la roca, los datos experimentales muestran un buen acuerdo con los perfiles teóricos de  $h(t)$ .

*Descriptores:* Imbibición; Flujo en medios porosos; Flujo de calor en medios porosos; Inestabilidades inducidas por tensión superficial.

PACS: 47.55.Mh; 44.30.+v; 47.20.Dr

## 1. Introduction

For nearly a century [1], isotherm imbibition in homogeneous porous media has been a topic of interest for scientists and engineers due to its inherent complexity and practical importance in many technological areas such as chromatography, textile and paper treatment, drying ink, enhanced oil recovery and metal wettability, among others [2–9]. It is well known that in a porous medium, the penetration kinetics of the wetting fluid frequently is characterized by the average penetration distance of the front,  $h(t)$ , which is measured on isotherm samples of sandstone or blotting paper, through the contrast between the dry and the imbibed (wet) zones. To our knowledge, imbibition under non isotherm conditions, for instance, when the porous sample is subjected to longitudinal temperature gradients, has not been previously considered. This type of capillary flow appears naturally, for instance, in oil and water reservoirs because they are under the action of the geothermal gradient or, in a forced way, during the injection of a fluid with a temperature either higher or lower than the *in situ* reservoir temperature [10–14]. In addition, imbibition under strong gradients also appears during the drying of porous media due to the existence of elevated fluid temperatures occurring in this type of a process [15]. The aim of this work is to build a model in order to understand imbibition into a porous medium under a constant temperature gradient,  $G$ .

To reach our goal, in the next Section we shall study theoretically the imbibition into a porous sample through the one-dimensional Darcy equation, which includes the driven capillary pressure and the hydrostatic pressure. In this type of equation, the influence of the temperature gradient on dynamic viscosity  $\mu$  and surface tension  $\sigma$  will be included explicitly through linear laws depending on temperature. The analytical solution of the resulting equation predicts an acceleration (deceleration) of  $h(t)$  with respect to the isotherm case. In Sec. 3, we show the results of a set of imbibition experiments in Berea sandstone under the action of  $G$ . Berea sandstone is a standard permeable, homogeneous rock commonly employed in experiments where well characterized and close-to actual conditions are required [16]. The evolution of  $h(t)$  was monitored in the rock by using digital video-recording. This technique allows us to measure  $h(t)$  very accurately. To measure the temperature profiles, in the rock during the experiments, an infrared camera was employed. Therefore, a fine overall temperature distribution on the rock was determined at every stage of the experiment. In particular, measurements in cases when  $G \neq 0$  enable us to note the existence, just at the corners of the sample, of a smooth deformation of the isotherms due to the existence of a thermal boundary layer. An order of magnitude analysis is given to determine the magnitude of these deformations and their influence on imbibition. Finally, in Sec. 4, the main conclusions and limitations of the present study are discussed.

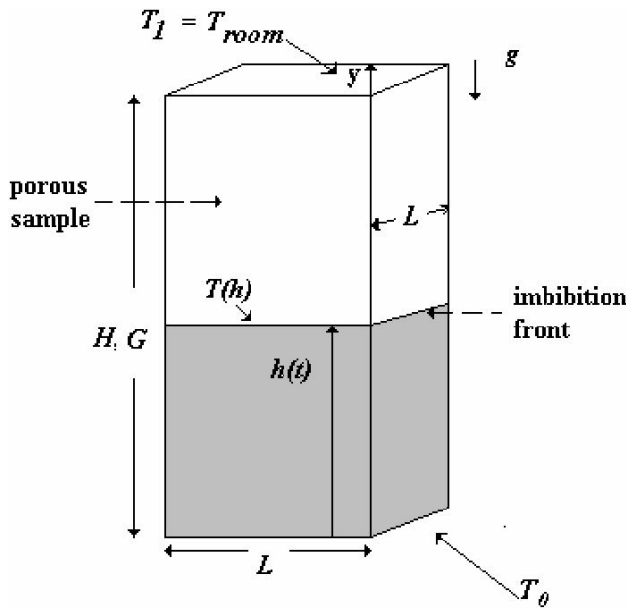


FIGURE 1. Schematic view of the imbibed region (grey zone) and the instantaneous imbibition front  $h(t)$ . The block has height  $H$  and cross sectional area  $L^2$ , is under the gravity field  $g$  and a longitudinal temperature gradient  $G = (T_1 - T_0)/H$ . Here,  $T_0$  is the temperature on the lower face and  $T_1$  is the temperature on the upper face.

## 2. Imbibition in the porous medium

Here, we study the imbibition into a porous medium of height  $H$  and cross sectional area  $L^2$ , which allows us to understand the penetration kinetics under temperature gradients. This model can, in fact, be extended to rectangular samples of typical dimensions  $L \times W$ ; however, the simplest geometrical model, particularly when the heat conduction problem is treated, is that of squared cross section. We first build a one-dimensional pressure drop equation, which considers that the capillary pressure  $p_c = -c_1\sigma(h)/d$  induces the motion and consequently the pressure drop  $\Delta p$ . Thus

$$-\frac{c_1\sigma(h)}{d} = \Delta p. \tag{1}$$

The quantity  $c_1$  is a dimensionless lumped constant which involves the wetting properties such as the angle of contact  $\theta$  and properties of the structure of the porous medium such as porosity,  $\phi$ . Moreover, the average pore diameter is  $d$ , and  $\sigma(h)$  is the surface tension at the averaged penetration distance,  $y = h(t)$  (see Fig. 1). The fluid flow through the homogeneous porous medium at low velocities is governed by the unidirectional Darcy law, which allows us to establish a relationship between the average filtration velocity  $\bar{v}$  and the pressure gradients

$$\bar{v} = -\frac{d^2}{c_2\mu(y(T))} \left[ \frac{dp}{dy} + \phi\rho g \right], \tag{2}$$

where  $p$  is the pressure;  $\mu(y(T))$  is the height-dependent dynamic viscosity, which under the gradient action, at different

heights, takes on different values because it depends on temperature;  $g$  is the gravity acceleration; and  $\rho$  is the fluid density. The density changes are small in comparison to changes of  $\mu$  and  $\sigma$  [17]. In Eq. (2), it is assumed that permeability  $K$  is related to the average pore diameter in the form  $K \sim d^2$  [5–7, 18], and therefore  $c_2$  is another dimensionless lumped constant which depends also on  $\phi$ . Rearranging Eq. (2), and using the fact that  $\bar{v} = dh/dt$ , the pressure drop is

$$\Delta p = \int_0^{h(t)} dp = -\frac{c_2}{d^2} \frac{dh}{dt} \int_0^{h(t)} [\mu(y(T))] dy - \phi\rho gh. \tag{3}$$

To integrate this latter, we allow the viscosity to depend on height, assuming a linear law, say,  $\mu(y(T)) = \mu_0 [1 + 1/\mu_0 (d\mu/dT)Gy]$ , where  $\mu_0$  is the viscosity at a reference value  $T = T_0$  and  $G = dT/dy$ , which in this work will be assumed as constant. After integration and substitution of  $\Delta p$  into Eq. (1), we obtain an implicit equation for the front evolution  $h(t)$  in the form

$$-\frac{c_1\sigma(h)}{d} = -\frac{c_2\mu_0}{d^2} \frac{dh}{dt} \left( h + \frac{\mu_0'G}{2\mu_0} h^2 \right) - \phi\rho gh, \tag{4}$$

where  $\mu' = (d\mu/dT)$ . Likewise, we can assume a linear law for surface tension,

$$\sigma(h(T)) = \sigma_0 [1 + 1/\sigma_0 (d\sigma/dT)Gh],$$

where  $\sigma_0$  is the surface tension at  $T = T_0$  and  $\sigma' = (d\sigma/dT)$  is the “temperature coefficient” [9]. Finally, the substitution of the relation for  $\sigma(h(T))$  into Eq. (4) yields the non-linear ordinary differential equation

$$\frac{c_1\sigma_0}{d} \left( 1 + \frac{\sigma_0'}{\sigma_0} h \right) - \phi\rho gh - \frac{c_2\mu_0}{d^2} \frac{dh}{dt} \left( h + \frac{\mu_0'G}{2\mu_0} h^2 \right) = 0, \tag{5}$$

which will be solved with the boundary condition  $h = 0$ , at  $t = 0$ . The differential equation can be expressed in a simpler form using the dimensionless variables  $\xi = h/h_0$  and  $\tau = t/t^* = c_1 d\sigma_0 t / (c_2 \mu_0 h_0^2)$ , where  $h_0$  is the equilibrium height reached by assuming isothermal imbibition and the balance between the hydrostatic and the capillary pressures; therefore,  $h_0 = c_1\sigma_0 / (\phi\rho gd)$ .

In addition, the following dimensionless viscosity and surface tension gradients are defined:

$$A = \frac{\mu_0'Gh_0}{2\mu_0}, \quad B = \frac{\sigma_0'Gh_0}{\sigma_0}. \tag{6}$$

Notice that  $A$  and  $B$  can have positive, negative or null values, depending on  $G$ . The resulting dimensionless differential equation becomes

$$1 + (B - 1)\xi - (\xi + A\xi^2) \frac{d\xi}{d\tau} = 0, \tag{7}$$

with  $\xi = 0$  at  $\tau = 0$ . Therefore, the solution of Eq. (7) is

$$\tau = \left[ \frac{B - A - 1}{(B - 1)^2} \right] \xi + \left[ \frac{A}{2(B - 1)} \right] \xi^2 + \left[ \frac{A - B + 1}{(B - 1)^3} \right] \ln [1 + (B - 1)\xi]. \quad (8)$$

Clearly, this solution shows a competition between the gradients  $A$  and  $B$  and, in a sense, they modulate the evolution of the front  $\xi(\tau)$  under temperature gradients. The isothermal case is immediately recovered when  $G=0$  ( $A=B=0$ ), in this case we obtain, from Eq. (8), the well known relation for imbibition in a porous medium under the gravity field [9, 19, 20]

$$\tau = -\xi - \ln(1 - \xi). \quad (9)$$

The law known as the Washburn law [19] (valid for very small penetration distance) is also recovered when  $\xi \ll 1$  because in this asymptotic case the solution is given either by  $\tau = \xi^2$  or, in dimensional form, by  $h^2 = [c_1 d \sigma_0 / (\mu_0 c_2)] t$ .

Generally speaking, the capillary penetration in the porous medium should be affected by the temperature, if the local temperature difference between the local bulk temperature of the liquid and the temperature of the most immediate grain can be neglected. This condition will be satisfied provided that the dimensionless relation  $(dh/dt)d/\kappa_l \ll d_g/d$  is valid [21], where  $\kappa_l$  is the liquid thermal diffusivity, and  $d_g$  is the grain average diameter. The quantity  $(dh/dt)d/\kappa_l \equiv Pe$  is the Peclet number and it compares the bulk transport of heat under forced convection (with velocity  $dh/dt$ ) respect to the heat transfer by conduction. Thus, a very small Peclet number refers to a very slow flow where heat conduction dominates. Consequently the previous imbibition model relies on these assumptions and the imbibition experiments to be discussed afterwards will be conducted following just these criteria. Furthermore, it will be discussed in detail in Sec. 4.

### 3. Experimental setup and isotherms in the rock

Prior to imbibition, the imposition on the overall rock of a steady, longitudinal temperature gradient was made as follows: the base of a rectangular dry rock (Berea sandstone) with dimensions as aforementioned (Fig. 1), was brought in to contact with a heat exchanger which maintained this part at a constant temperature  $T = T_0$ . The other faces of the rock are in contact to air, which was maintained at a constant temperature  $T = T_1$ . In this case the rock, with thermal diffusivity  $\kappa_p$ , can be seen as a fin which, after the diffusive time  $t_D = H^2/\kappa_p$ , reaches approximately the temperature distribution  $T(y) \simeq T_0 + Gy$  [21] where  $G = (T_1 - T_0)/H$ .

Typical experiments were conducted on bold rocks with size  $H=0.085$  m height and  $L=0.05$  m length and the physical properties of the Berea were density  $\rho_p=2300$  kg/m<sup>3</sup>, thermal diffusivity  $\kappa_p=0.011 \times 10^{-4}$  m<sup>2</sup>/s, permeability  $K=500$  mD, porosity  $\phi=20\%$  and thermal conductivity

$k_p=0.9$  cal/(m s K). Therefore, the diffusive time to achieve a longitudinal temperature gradient was  $t_D=1.8$  h. However, measurements of the steady-state temperature distributions were made after 4 h, and we brought the rock to the exchanger. Very accurate temperature field measurements (thermographies) were made by using an infrared camera model FLiR Thermacam-PM595 with a resolution of 0.1 K. Typical overall temperatures, measured on any face of the rock, are shown in Fig. 2a for the case  $G>0$  and in Fig. 2b for the case  $G<0$ . The case  $G>0$ , was obtained by making  $T_0=295.2$  K and  $T_1=299.2$  K, consequently  $G_+=47.059$  K/m. When  $G<0$ ,  $T_0=307$  K and  $T_1=303$  K and  $G_-=-47.059$ . This temperature range, above room temperature ( $T_{room} = 295.2$  K), was selected so as to have a clear contrast between the isotherms by using the infrared camera. Notice that  $G_+ = |G_-| = 47.059$  K/m. The case when  $G = 0$  was obtained for  $T_{room}=295.2$  K.

We can perform an order of magnitude analysis of the shape of the isotherms depending on the sign of the gradient. We notice in Fig. 2a that the isotherms (equal gray-tone regions) when  $G>0$  have a small curvature, while the curvature (folding) of the isotherms when  $G<0$  is very small, as is evident from Fig. 2b. This peculiar phenomenon is due to the existence of a thermal boundary layer which plays an

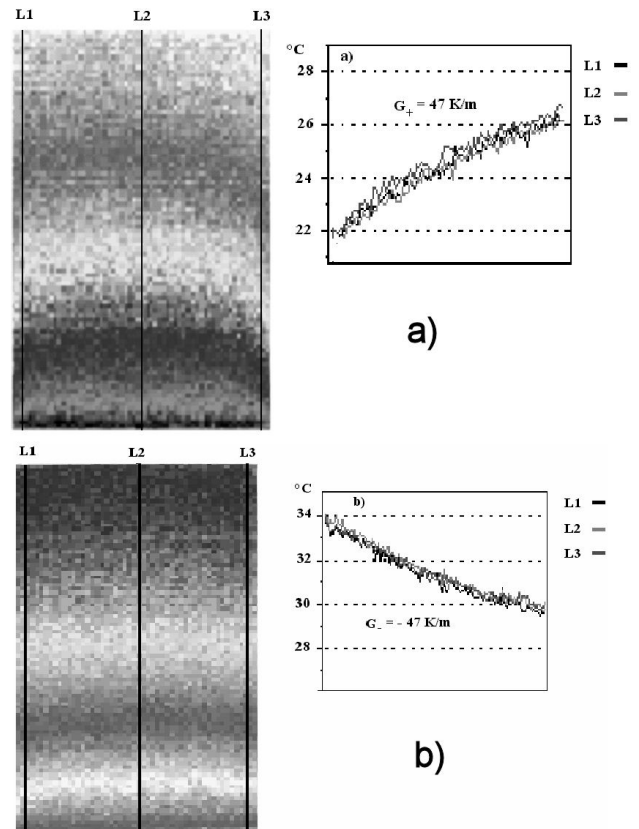


FIGURE 2. a) Typical thermography of a face of the dry rock (Berea sandstone) and plot of the temperature as function of  $y$  for  $G > 0$  and b) typical thermography of the same type of rock and plot of the temperature as a function of  $y$  for  $G < 0$ .

important role in cases where a gradient is imposed in bold rocks, as will be shown afterwards. The estimation of the size of the thermal boundary layer is important to ensure in the experiments that the temperature gradient is homogeneous at any place of the rock excepting the corners.

When the gradient has been imposed on the rock, the density of the air close to the rock surfaces changes because of the increased temperature. A bouyancy-driven convective flow is developed within the viscous boundary layer of width  $\delta$  (see Fig. 3). We consider that the air has density  $\rho_g$ , dynamic viscosity  $\mu_g$ , thermal volume expansion coefficient  $\beta_g$  and thermal conductivity  $k_g$ . The velocity  $u$  of the convective flow in the boundary layer is obtained through the energy equation where the convective and bouyance terms are the dominant ones. Hence,

$$\rho_g u^2 \sim \rho_g g H \beta_g \Delta T, \tag{10}$$

where the temperature change in the boundary layer is of the same order as that occurring in the overall length,  $H$ . Therefore, the convective velocity is

$$u \sim (g H \beta_g \Delta T)^{1/2}. \tag{11}$$

The width of the boundary layer,  $\delta$ , is evaluated by considering the viscous damping of the flow

$$\rho_g \frac{u^2}{H} \sim \mu_g \frac{u}{\delta^2}. \tag{12}$$

Using relation (11) in (12) we obtain

$$\delta \sim \left( \frac{\mu_g H}{\rho_g u} \right)^{1/2} \sim H \left( \frac{\mu_g^2}{\rho_g^2 g \beta_g \Delta T H^3} \right)^{1/4} \sim \frac{H}{Gr^{1/4}}, \tag{13}$$

where  $Gr = \rho_g^2 g \beta_g \Delta T H^3 / \mu_g^2$  is the Grashof number. On the other hand, the heat flux  $q_g$  is given by

$$q_g \sim k_g \frac{\Delta T}{\delta} \sim k_g \frac{\Delta T}{H} Gr^{1/4}, \tag{14}$$

where Eq. (13) has been used. On the rock, close to any corner, it is observed in Fig. 2b that the isotherms have a small deformation. We assume that it is due to the transverse heat flux,  $q_p$ , given by

$$q_p \sim k_p \frac{\Delta_\chi T}{L}, \tag{15}$$

where  $\Delta_\chi T$  is the temperature variation in a zone of length  $\chi$  (see Fig. 3). Both heat fluxes  $q_g$  and  $q_p$  are of the same order of magnitude, therefore

$$k_p \frac{\Delta_\chi T}{L} \sim k_g \frac{\Delta T}{H} Gr^{1/4}. \tag{16}$$

The relative change between the isotherms is given by

$$\frac{\Delta_\chi T}{\Delta T} \sim \frac{k_g}{k_p} \frac{L}{H} Gr^{1/4}. \tag{17}$$

To estimate the Grashof number and the magnitude of the deviation of the isotherms, respect to horizontal ones for  $G < 0$ , we used  $\rho_g = 1.14 \text{ kg/m}^3$ ,  $\mu_g = 18.87 \times 10^{-6} \text{ Pa s}$ ,  $k_g = 0.006 \text{ cal/(m s K)}$ ,  $\beta_g = 3.26 \times 10^{-3} \text{ K}^{-1}$ , corresponding to  $T_0 = 307 \text{ K}$  for which  $Gr^{1/4} = 23.12$ . Finally, from Eq. (17) we found that

$$\frac{\Delta_\chi T}{\Delta T} \sim 0.11, \tag{18}$$

a result that indicates that the deviation of the isotherm close to any corner is of around 10%. Such a result is in good agreement with the deviations measured close to the corner,

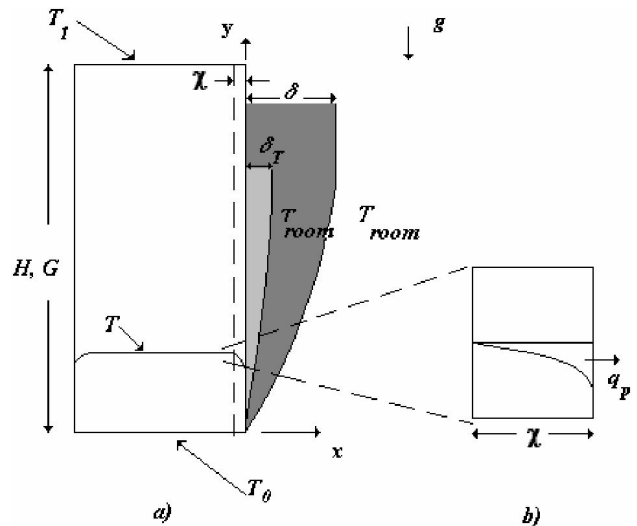


FIGURE 3. a) Thermal ( $\delta_T$ ) and viscous ( $\delta$ ) boundary layers (outside the block) and isotherms on the block which are deformed close to the corners. b) Detailed view of the zone where isotherms are folded. It is assumed that just in those zones, of length  $\chi$ , isotherms are deformed and produce a heat flow  $q_p$ .

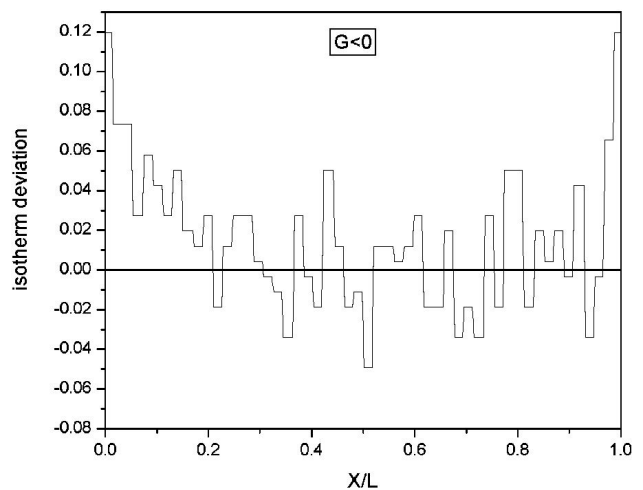


FIGURE 4. Typical plot of the temperature deviation obtained from Fig. 2b, *i.e.*, when the rock has a negative gradient ( $G < 0$ ). In this case maximum deviation occurs close to the rock corners ( $x/L = 0, 1$ ). This deviation is around 10%, as it was determined through the estimation of the quantity  $\Delta_\chi T / \Delta T$  (Eq. (18)).

as is shown in Fig. 4. The case of  $G > 0$  is related to an other type of thermal boundary layer which originates in the lower part due to the higher weight of air in this region. An estimate of the deviation in this case can be found in a similar way.

Another very important aspect related to the local temperature variations at the corners is that these variations do not change the overall temperature at a given height. In fact, two independent procedures were conducted in order to prove it: First.- Measurements were made at several inner points, along horizontal holes drilled in the sandstone using thermocouples, with a resolution of around 0.01 K. In general, no horizontal temperature gradient was detected along the hole. Second.- By using the thermographies (Figs. 2a and 2b), the zones where the isotherms were bent and located at around 6% of  $L$  in cases where  $G < 0$  and 12% of  $L$  in cases where  $G > 0$ . Thus, the percentage of area where the isotherms have a different value than that of their mean value was 1% when  $G < 0$ , and 5% when  $G > 0$ . Both facts lead us to conclude that the temperature distribution on the rock complies, in fact, with the profile  $T(y)$  given above except in very small zones at the corners, and so the heat conduction problem in the rock is essentially one-dimensional.

#### 4. Imbibition experiments

While the temperature gradient was imposed on the rock, a deionized-water reservoir was located at the bottom, alongside the heat exchanger, in order to have the same temperature as the lower part of Berea, *i.e.*,  $T_{liquid} = T_0$ . To induce spontaneous imbibition, the sandstone was gently dipped into the water reservoir and the imbibition process was video recorded using a CCD camera with a recording frequency of 30 frames per second. After, that each frame was fed into a computer as a digital image with a size of 480 pixels wide  $\times$  720 pixels high and a 256 gray scale. By controlling the illumination intensity and the shutter of the video recorder, by a simple filtering process it is possible to extract the image of the front and the measurement scale. The calibration used to measure the instantaneous imbibition front on each frame was  $1 \times 10^{-4}$  m/pixel in the vertical direction. By applying this procedure, we measured the imbibition front,  $h$ , as a function of the elapsed time,  $t$ , with a spatial resolution of 0.1 mm.

Despite the imbibition process, the infrared camera did not detect changes in the temperature distribution in the rock. As mentioned in the Sec. 2, this occurs because, as water rises into the rock, it achieves almost immediately reaches the temperature of the rock. Our experimental measurements give a maximum Peclet number of  $Pe = 0.43$ , and the ratio  $d_g/d = 126.49$ , *i.e.*, the condition of neglecting local temperature difference between the grains of the porous medium and the liquid ( $Pe \ll d_g/d$ ), is satisfied. In the evaluation of  $Pe$  and  $d_g/d$  we used the highest value of the imbibition velocity measured in the experiments ( $dh/dt = 40 \times 10^{-3}$  m/s),  $d_g = 200 \mu\text{m}$  (measured through a  $10\times$  microscope) and the

value of the pore size  $d$  was calculated through the correlation  $d \sim (K/\phi)^{1/2} = 1.58 \mu\text{m}$  [5–7, 18].

To construct the dimensionless graphs given by Eq. (8) that fit the experimental data, we need to know the dependence of  $\mu$  and  $\sigma$  on  $T$ . Tabulated values of these quantities were taken from Lide [17] and used in Eqs. (6) and (8). Moreover, these data match well the linear expansions of  $\mu$  and  $\sigma$  given above. In this context, values of  $\mu'$  and  $\sigma'$  in the temperature range here considered are  $|\mu'| = 1.7 \times 10^{-5}$  N s/m<sup>2</sup>K and  $|\sigma'| = 1.47 \times 10^{-4}$  N/m K. The water density used was  $\rho = 998$  kg/m<sup>3</sup>. The temperature profiles shown in Fig. 2 deviate slightly from the ideal linear profile  $T(y) = T_0 + Gy$ ; however, this last approximation was maintained because we considered a spatially-averaged value of  $G$ . Moreover, due to the existence of small differences between the temperature at the middle part ( $L/2$ ) and those at the corners, the values of the spatially-averaged imbibition profiles given below were taken just in the middle section. Given these facts, three cases were analyzed: In the first case a negative temperature gradient was established  $G_- = -47$  K/m (the subscript indicates the sign of the gradient); in the second one, a positive gradient  $G_+ = 47$  K/m was imposed; and the last was a case in which  $G = 0$ . For this last case, the temperature of the rock and water was room temperature  $T_{room} = 295.2$  K. As mentioned above, in order to compare the results between negative and positive gradients, the condition  $|G_-| = G_+$  was selected.

In Fig. 5, we show dimensionless plots of the averaged imbibition heights as  $\xi$  versus  $\tau$ . These plots were obtained from Eq. (8) for cases when  $G \neq 0$  and from Eq. (9) for  $G = 0$ . In the same figure, we also show the experimental data for all values of  $G$ . The lumped constants  $c_1$  and  $c_2$  appear in the dimensional form of Eqs. (8) and (9) as a ratio  $c = c_1/c_2$ . The value of  $c$  for each value of  $G$  was determined with the best fit of the theoretical profile to the corresponding set of data (symbols). This procedure allowed us to find that  $c = 4.2 \times 10^{-2}$  when  $G = 0$ ,  $c = 4.4 \times 10^{-2}$  for  $G > 0$  ( $G_+ = 47$  K/m) and  $c = 5.3 \times 10^{-2}$  for the case  $G < 0$  ( $G_- = -47$  K/m). These values are of the same order of magnitude, but they are different among themselves because they are linked to the value of the angle of contact  $\theta$  which changes with temperature, as is shown from simple experiments in circular capillaries [22]. The characteristic height and time used in the normalization were  $h_0 = 4.6$  m and  $t^* = 4.2 \times 10^6$  s, respectively. Those quantities were obtained using fluid and rock data at  $T_0 = 295.2$  K.

The main result in the context of imbibition under temperature gradients is that there are important changes during the time evolution of the fronts. As can be seen from Fig. 5, imbibition in the case in which  $G < 0$  is faster than the cases for which  $G > 0$  and  $G = 0$ . The reason for this behavior is that in many liquids, including water, the dynamic viscosity and surface tension decrease when  $T$  increases. Both effects, including the magnitude and sign of the gradient, are considered in the dimensionless gradients  $A$  and  $B$  and therefore these quantities have an important influence on  $\xi(\tau)$ , which

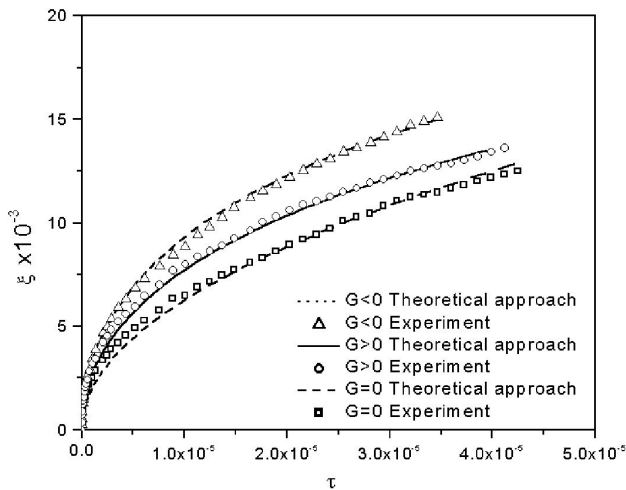


FIGURE 5. Dimensionless plot of the theoretical profiles  $\xi(\tau)$  (curves) and experimental points (symbols) for the several values of  $G$  considered in this work:  $G=0$  where  $T_o=T_1=T_{room}=295.2$  K ( $\square$ ),  $G<0$  where  $G_-=-47$  K/m ( $\triangle$ ), and  $G>0$  where  $G_+=47$  K/m ( $\circ$ ). Symbols are the size of the error bars.

is given implicitly in Eq. (8). Theory and the experiments allow us to show that imbibition under temperature gradients is accelerated/decelerated depending on the thermal conditions of the porous medium and the fluid involved.

## 5. Conclusions and remarks

In this investigation, the problem of imbibition into a porous material under temperature gradients was analyzed. We found that the theoretical predictions, which are applicable for  $Pe \ll d_g/d$ , are in good agreement with the experimental results. The main considerations in the theoretical treatment were the imposition of a constant temperature gradi-

ent and those related to linear dependence of dynamic viscosity and surface tension on the temperature. Through experiments, complex temperature distributions were observed when a constant temperature was imposed at the base of the rock. When this temperature was different from the ambient temperature, a thermal boundary layer was formed. This layer modified the overall temperature distribution, mainly the shape of the isotherms in regions close to the corners. In spite of this, well defined spatial temperature fields were imposed on the rock, and it was found that temperature gradient has an important influence on the spatially-averaged imbibition rates. In summary, the main result of this work is the acceleration/deceleration of the imbibition front depending on the sign of temperature gradient and the way in which the dynamic viscosity and surface tension change with  $T$ . Experiments using deionized water and Berea sandstone were performed to corroborate the validity of the one-dimensional model. It was observed that, under the action of a negative gradient, the time to reach a height  $\xi$  is around half the time that for the isotherm case. More detailed and complex studies can be carried out to model other interesting aspects of imbibition, for example the existence of interfacial instabilities (fingers), changes in the rock saturation, wetting at very high temperatures, etc. However, the essence of the problem appears to be contained in the simple model presented here. Further studies related to imbibition using fluids of importance in the petroleum industry, such as oil and brine, are now in progress.

## Acknowledgments

The authors acknowledge the careful revision given to this work by the anonymous reviewer. This work has been supported by PIMAC-IMP under project D.0330.

1. J.M. Bell and F.K. Cameron, *J. Phys. Chem.* **10** (1906) 658.
2. M.C. Cross and P.C. Hohenberg, *Rev. Mod. Phys.* **65** (1993) 851.
3. O. Zik, T. Kustanovich, E. Moses, and Z. Olami, *Phys. Rev. E* **58** (1998) 689.
4. I. Prezon, G. Bourgain, and D. Quere, *J. Colloid Interface Sci.* **173** (1995) 319.
5. J. Bear, *Dynamics of Fluids in Porous Media* (Dover, New York 1988).
6. G.I. Barenblatt, V.M. Entov, and V.M. Ryzhik, *Theory of Fluid Flows Through Natural Rocks* (Kluwer, Dordrecht, 1990).
7. F.A.L. Dullien, *Porous Media, Fluid Transport and Pore Structure* (Academic Press, San Diego, 1991)
8. N.R. Morrow and G. Mason, *Current Opinion Colloid Interface Sci.* **6** (2001) 321.
9. N. Eustathopoulos, M.G. Nicholas, and B. Devret, *Wettability at High Temperatures* (Pergamon Press, Oxford, 1999).
10. L.W. Lake, *Enhanced Oil Recovery* (Prentice Hall, New Jersey, 1989).
11. T. Babadagli, *J. Pet. Sci. Eng.* **14** (1996) 197.
12. A. Donmez, "Investigation of the effect of temperature on heavy oil recovery by imbibition mechanism," paper SPE 37555 presented at the 1997 SPE International Thermal Operations and Heavy Oil Symposium, California, 10-12 February 1997.
13. M.E. Chimenti and H.L. Najurieta, "Influence of temperature and interfacial tension on spontaneous imbibition process," paper SPE 53668 presented at the 1999 SPE Latin American and Caribbean Petroleum Engineering Conference, Caracas Venezuela, 21-23 April 1999.
14. T. Babadagli, *J. Pet. Sci. Eng.* **33** (2002) 223.
15. F. Plourde and M. Prat, *Intl. J. Heat Mass Transfer* **46** (2003) 1293.
16. P-E. Oren and S. Bakke, *J. Pet. Sci. Eng.* **39** (2003) 177.

17. D.R. Lide, *Handbook of Chemistry and Physics* (CRC Press, San Francisco, 1996).
18. L.L. Popovich, D.L. Feke, and I. Manas-Zloczower, *Powder Technol.* **104** (1999) 68.
19. E.W. Washburn, *Phys. Rev.* **17** (1921) 273.
20. T.L. Staples and D.G. Shaffer, *Colloids and Surfaces A: Physicochem. Eng. Aspects* **204** (2002) 239.
21. A. Bejan, *Heat Transfer* (John Wiley, New York, 1993).
22. T.S. Sammarco and M.A. Burns, *AIChE J.* **45** (1999) 350.